RHEOLOGY OF BLOOD IN SMALL VESSELS

M. Scott and G. Tenti

Department of Applied Mathematics
University of Waterloo, Waterloo, Ontario N2L 3G1, Canada

Abstract. Blood is a dense suspension of flexible red blood cells. In response to a background flow, these cells are distributed inhomogeneouesly throughout the vessel. As a result, material properties that are well-defined in homogeneous fluids, such as viscosity, are no longer so, and depend upon the flow geometry along with the particle properties. Using a simple model that accounts for the steady-state particle distribution in vessel flow, we derive an expression for the effective viscosity of blood and the suspension flow velocity field.

1 Introduction

Whole blood is a concentrated suspension of (predominantly) red blood cells - occupying $> 95\%$ vol. of the particulate, and 45% vol. of the total volume. The mathematical modeling of blood rheology is complicated by the description of the microstructure that develops as particles are redistributed in the background flow. The inhomogeneous particle distribution leads to a variation of the local suspension properties across the vessel, and consequently, models used to describe homogeneous fluids no longer apply, even under the most benign laminar flow conditions.

The inhomogeneous arrangement of red blood cells in flowing whole blood results in surprising rheological behavior - the most famous of which is the Fahraeus-Lindqvist effect [13]. When blood is forced through a narrow glass tube, it becomes comparatively easier to maintain the flow as the tube diameter decreases than it would be to maintain the flow of an analogous homogeneous fluid. That is to say, the effective viscosity of blood decreases as the tube diameter decreases. Furthermore, while homogeneous fluids display a parabolic Poiseuille velocity distribution across the vessel (for sufficiently low Reynolds number), blood exhibits a plateau maximum along the vessel axis typical of plug flow. Experiments suggest that the width of this uniform-velocity core depends upon many factors, including cell deformability, solute

volume fraction, viscosity of the suspending medium, tube radius and the pressure drop along the tube[14, 18].

There are several empirical models that are used to quantify these characteristic flow anomalies. The constitutive equation derived by Casson [5] to explain the non-Newtonian rheology of printer's ink is often used in the study of blood flow [7, 33]. In Casson's model, the non-linear relationship between the stress and the rate of shear contains two unknown parameters: the yield-stress and the Casson limiting viscosity. Both parameters are notoriously difficult to quantify experimentally with any great consistency and often experiments performed with different types of viscometer will arrive at parameter values that differ by $10 - 20\%$ [7]. A deeper problem with the Casson approach is that uniform particle distribution is implicit in the derivation of the model, with the non-Newtonian characteristics coming from the aggregation of particles. Yet it is clear from the work by Chien [8] that aggregation plays a minor role at physiological flow rates because aggregating and non-aggregating suspensions behave identically for shear rates above 3 s^{-1} in a Couette viscometer.

A second class of empirical models explicitly account for the particle microstructure by viewing blood as a layered fluid [19] - with a highly viscous core surrounded by a lubricating annulus of cell-free plasma. In these two-fluid (or core-annular) models, the width of the lubricating layer is a free parameter used to fit experimental data. In principle, there is no limit to the number of layers into which the flow can be divided, with the width and viscosity of each left free to fit with experimental data. Unfortunately, the layered models provide no mechanism for the particle distribution, and so are of limited predictive value.

More fundamental approaches have been developed to model suspension flow. Microhydrodynamic models [2, 9, 20] follow the methodology of the kinetic theory of gases, deriving macroscopic properties from the statistical moments of underlying microscopic distributions. The formalism is unwieldy, however, and it is difficult to incorporate the effect of bounding walls. In particular, pressure-driven pipe flow does not seem to have ever been treated in this way [20]. Currently, suspension flows are popularly visualized by numerical simulations [32, 38], although results derived by numerical methods retain an empirical quality, with the detailed data often interpreted by scaling arguments or described with fitting functions.

Here we shall adopt a more phenomenological approach used by others to model the rheology of dilute emulsions [21, 24]. We describe a model that begins with an examination of the mechanisms underlying particle migration in the background flow to provide an expression for the steady-state effective viscosity and velocity profiles for constant and pulsatile tube flow. We find that in the limit of vanishing Péclet number, the effective viscosity reduces to Einstein's relation including a correction due to flow induced cell migration. Furthermore, the expressions derived are essentially dependent upon the confining geometry and we conclude that the measured properties

of a suspension are therefore dependent upon the viscometer used to make the measurements. (For a more detailed analysis of a variety of viscometer geometries, see [35].)

2   Mathematical model

Our chief aim is to connect the particle microstructure with the macroscopic suspension flow. Our approach will be to describe the particle volume fraction ϕ using mass-conservation, and the creeping flow equations for the overall suspension velocity $\vec{u}$, connecting the two disparate length scales with a phenomenological constitutive relation for the local fluid stress $\tau(\phi)$ (Figure 1). Here and henceforth we refer all physical quantities to a standard cylindrical coordinate system (r, θ, z) with the z-axis along the vessel axis.

In order to proceed, we require a suitable geometrical representation of the red blood cells. As is well known, at rest these are biconcave disks about 8 μm is diameter and 2 μm thick. Their shape is difficult to model explicitly, although some shape-based rheological models have been developed [29]. Here, we make the simplification that in flow they behave like spherical droplets of immiscible fluid [1, 14, 40]. We can then take advantage of the work of Chan and Leal [6] who studied the problem of the migration of a fluid drop in a unidirectional shear flow, under the assumption that both the suspending fluid and the fluid inside the drop can be adequately modeled as second-order fluids. In fact, we will need only a special case of this theory, because blood plasma behaves like a Newtonian fluid.

2.1   Microscopic particle distribution

Consider a control volume V of fixed shape moving with the background fluid flow. There is some volume fraction of V occupied by particles, called ϕ. Invoking a conservation of mass within the control volume, the particle volume fraction ϕ is governed by the conservation equation,

$$\frac{\partial \phi}{\partial t} = -\vec{\nabla} \cdot \vec{J},$$

where $\vec{J}$ is the flux of particles across the surface of the control volume. There are two primary mechanisms driving flux across the surface – convective flux and diffusive flux.

2.1.1   Convective flux

A neutrally buoyant hard sphere in creeping Newtonian flow will not show any cross-stream migration [3]. Convective flux can only be realized if some term (e.g. nonlinearity) is introduced into the creeping flow equations to break the symmetry [26]. This is the case, for example, when the Reynolds number is small but the nonlinear inertia terms contribute asymptotically to
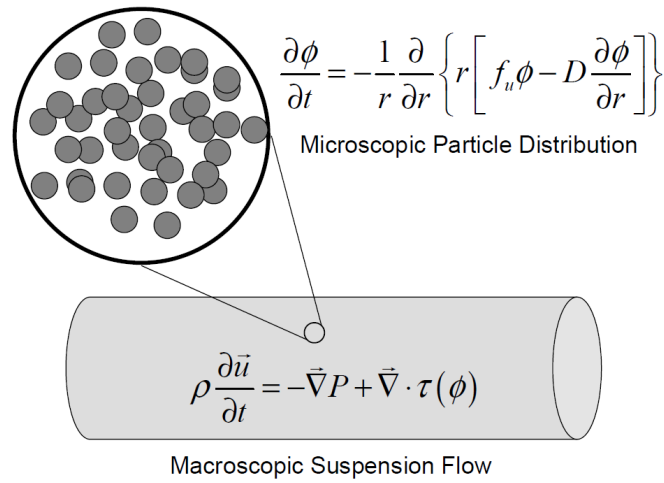
$$\frac{\partial \phi}{\partial t} = -\frac{1}{r}\frac{\partial}{\partial r}\left\{ r\left[f_u \phi - D\frac{\partial \phi}{\partial r}\right]\right\}$$

Microscopic Particle Distribution

$$\rho\frac{\partial \vec{u}}{\partial t} = -\vec{\nabla}P + \vec{\nabla}\cdot\tau(\phi)$$

Macroscopic Suspension Flow

Figure 1: **Connecting the macroscopic flow with the suspension microstructure**. Blood is largely a suspension of red blood cells that are arranged non-uniformly in response to a background flow. The microscopic particle volume fraction ϕ is connected to the resultant suspension flow velocity $\vec{u}$ by the local stress tensor $\tau(\phi)$. The particle volume fraction ϕ is governed by a advection-diffusion equation, where f_u is the cross-stream migration velocity (see Eq. (2)) and D is the flow-dependent diffusion constant.

the steady-state, or when the solvent is treated as a weakly non-Newtonian fluid whose constitutive equation introduces the symmetry breaking non-linearity. Most important to the present study is the convective flux arising from drop deformability, which transforms the mathematical model into a free boundary-value problem in which the location of the surface of the deformed drop has to be determined as part of the solution. The resulting symmetry-breaking condition can be exploited by means of perturbative techniques by assuming that the spherical shape of the particle is slightly altered by hydro-dynamic interactions with the walls and by the stretching of the surface in the flow shear-gradient. For Poiseuille flow, with small ratio of particle-to-tube radius, shear-gradient effects dominate and particle migration is predicted even in unbounded flows.

Using an approach similar to Goddard and Miller's [15] work on a deformable sphere in unbounded linear shear flow, Chan and Leal [6] derive the velocity field around a deformable sphere in bounded, unidirectional quadratic shear flow and predict that the background shear gradient and bounding walls lead to an induced droplet migration toward the tube axis. Their solution proceeds as an asymptotic expansion of the free-boundary creeping flow problem in inverse powers of the particle deformability δ, with

$$\delta = \frac{a \eta_0 G}{\sigma}.$$

Here a is the particle radius, η_0 is the plasma viscosity, G is the average shear rate across the vessel, and σ is the interfacial tension of the particle. It follows that δ represents an estimate of the importance of viscous versus surface tension effects, and measures the degree of nonlinearity introduced by the free boundary conditions. The convective flux term is then given by

$$\vec{J}_{\text{conv}} = \phi f_u(r) \hat{e}_r,$$

where $f_u(r)$ is the cross-stream migration velocity (given below by Eq. 2) and $\hat{e}_r$ is the unit vector in the radial direction.

Following Chan and Leal [6], we consider a simplified and symmetric vessel geometry, where the down-tube length z is large compared with other length-scales in the problem (eg. z is on the order of millimeters). As a result, functional dependence on the down-tube distance z and the azimuthal angle θ are dropped from the governing equations.

2.1.2   Diffusive flux

There will also be a component of the flux due to collisions between particles, modeled by Fick's law,

$$\vec{J}_{\text{diff}} = -D\vec{\nabla}\phi,$$

where D is the diffusion coefficient. The diffusion may be spatially dependent for inhomogeneous concentrated suspensions, including restricted motion due

to cage effects [10] or asymmetric collisions in the shear flow [24, 28]. Here we assume that D is constant in space, though it may be dependent upon averaged quantities such as the flow rate and initial particle volume fraction.

In principle the total flux $\vec{J}$ will contain contributions arising from additional mechanisms, such as the electrostatic repulsion between the vessel walls and the particle surface, sedimentation, *etc.*, but we will only consider the convective and diffusive contributions discussed above. The conservation equation for the particle volume fraction then reads,

$$\frac{\partial \phi}{\partial t} = -\vec{\nabla} \cdot \left[\phi f_u(r) \hat{e}_r - D\vec{\nabla}\phi \right],$$

or, in cylindrical coordinates,

$$\frac{\partial \phi(r,t)}{\partial t} = -\frac{1}{r}\frac{\partial}{\partial r}\left\{ r\left[\phi(r,t)f_u(r) - D\frac{\partial \phi(r,t)}{\partial r} \right]\right\}. \tag{1}$$

Chan and Leal [6] have determined the migration velocity of an immiscible droplet suspended in a laminar tube flow, using an asymptotic expansion in the droplet deformability. The first term in this expansion provides an expression for $f_u(r)$ in a 3-dimensional Poiseuille flow (cf. Eq. (6.10) in the original article),

$$f_u(r) = -2F[\kappa]\frac{\eta_0 V_{\max}^2}{\sigma}\left(\frac{a}{R}\right)^3\left(\frac{r}{R}\right), \tag{2}$$

Here, $V_{\max}$ is the velocity of the background flow at the axis, σ is the interfacial tension, a is the radius of the droplet, R is the radius of the vessel, and $F[\kappa]$ is a function of the ratio $\kappa = \hat{\eta}/\eta_0$ of the viscosity inside the droplet $\hat{\eta}$, and the viscosity of the suspending fluid η_0,

$$F[\kappa] = \frac{3}{14}\left[\frac{16+19\kappa}{(2+3\kappa)^2}\frac{1-\kappa-2\kappa^2}{(1+\kappa)^2}\right]$$

$$+ \left[\frac{(10+11\kappa)}{140}\frac{8-\kappa+3\kappa^2}{(1+\kappa)^2(2+3\kappa)}\right].$$

The internal viscosity of the droplet $\hat{\eta}$ is a measure of the resistance offered to the motion of fluid within. The red blood cells, however, do not have a homogeneous internal structure, and so we must ask what meaning $\hat{\eta}$ can have in the context of a biological cell. It is not enough to lyse the cell, and measure the viscosity of the cell contents. The relevance of the internal viscosity to the migration velocity comes from the development of internal circulation patterns that dissipate energy [39]. The rugged internal architecture of the cell provides strong resistance to flow in the interior. It seems appropriate, then, to model the internal environment of the red blood cell as a highly viscous fluid, taking $\hat{\eta}$ asymptotically large (and constant) in Eq. (3), to arrive at $F[\kappa] \to 11/140$ as $\kappa \propto \hat{\eta} \to \infty$, or

$$f_u(r) = -2\frac{11}{140}\frac{\eta_0 V_{\max}^2}{\sigma}\left(\frac{a}{R}\right)^3\left(\frac{r}{R}\right). \tag{3}$$

Because the perturbation expansion of Chan and Leal assumes $\kappa \ll \mathcal{O}(1/\delta)$, the limit $\kappa \to \infty$ must therefore be interpreted as $\mathcal{O}(1) \ll \kappa \ll \mathcal{O}(1/\delta)$, with particle deformability $\delta \to 0$. Renormalizing time with respect to the rate of diffusion, $\hat{t} = \frac{D}{R^2}t$, and the radial distance by the vessel radius, $\hat{r} = \frac{r}{R}$, the particle conservation Eq. 1 reads

$$\frac{\partial \phi}{\partial \hat{t}} = \frac{1}{\hat{r}} \frac{\partial}{\partial \hat{r}} \left\{ \hat{r} \left[2\varepsilon \hat{r} \phi + \frac{\partial \phi}{\partial \hat{r}} \right] \right\}, \tag{4}$$

where the dimensionless parameter ε play the role of a Péclet number, and characterizes the ratio of the magnitude of the convective flux to the magnitude of the diffusive flux,

$$\varepsilon = \frac{11}{140} \frac{V_{\max}^2}{\sigma} \frac{\eta_0 a}{D} \left(\frac{a}{R}\right)^2. \tag{5}$$

Alternatively, the parameter ε can be thought of as a measure of the inhomogeneity of the steady-state particle distribution, because $\varepsilon = 0$ corresponds to the diffusion dominated regime, and therefore a homogeneous steady-state particle distribution. Consequently, we call ε the *inhomogeneous Péclet number*.

The steady-state solution of Eq. 4 is reached when the convective and diffusive flux balance. Integrating the right-hand side of Eq. 4 once, and enforcing zero flux across the axis, we arrive at the first-order ordinary differential equation,

$$\frac{d\phi^{ss}}{d\hat{r}} = -2\varepsilon \hat{r} \phi^{ss};$$

the steady-state particle distribution $\phi^{ss}(r)$ is therefore Gaussian,

$$\phi^{ss}(r) = C_0 \exp\left[-\varepsilon \hat{r}^2\right].$$

The integration constant C_0 is determined by enforcing the conservation of the total particle mass. With the initial particle volume fraction ϕ_0, conservation of the total mass requires that

$$\int_0^1 \hat{r} \phi_0 \, d\hat{r} = \frac{\phi_0}{2} = \int_0^1 \hat{r} \phi^{ss}(\hat{r}) \, d\hat{r}, \tag{6}$$

or,

$$C_0 = \frac{\varepsilon \phi_0}{1 - e^{-\varepsilon}}.$$

Equation 6 tacitly assumes that the particle packing along the axis can be arbitrarily tight. That is not the case, and while the particle density must certainly be less than 1, in practice complete packing is never achieved. Let $\phi_{\max}$ be the maximum volume fraction possible, then Eq. 6 holds as long as $C_0 \leq \phi_{\max}$. If a completely packed core develops at the axis, extending some

distance $\hat{r}_c$ from the center line, the steady-state volume fraction distribution $\phi^{ss}(\hat{r})$ will then be piece-wise defined,

$$\phi^{ss}(\hat{r}) = \begin{cases} \phi_{\max} & 0 \leq \hat{r} \leq \hat{r}_c \\ \phi_{\max} \exp\left[-\varepsilon(\hat{r} - \hat{r}_c)^2\right] & \hat{r}_c < \hat{r} \leq 1 \end{cases},$$

where now $\hat{r}_c$ is determined by the conservation of mass,

$$\int_{\hat{r}_c}^1 \hat{r}\phi_0 \, d\hat{r} = \phi_{\max} \int_{\hat{r}_c}^1 \hat{r} \exp\left[-\varepsilon(\hat{r} - \hat{r}_c)^2\right] \, d\hat{r}$$

$$= \frac{\phi_0 - \phi_{\max}\hat{r}_c^2}{2},$$

although the equation is transcendental and must be solved numerically.

2.2   Macroscopic suspension flow

To connect the steady-state particle distribution ϕ^{ss} with the dynamics of the overall flow velocity u, we postulate a generalized Newtonian constitutive equation [31] for the fluid stress τ,

$$\tau(\hat{r}) = \eta_\phi \frac{\partial u}{\partial \hat{r}},$$

where η_ϕ is the effect of the particle volume fraction ϕ on the local viscosity of the suspension. We leave the form of η_ϕ undefined for the moment, except to note that in the steady-state, η will depend upon the radial distance only: $\eta_\phi(\hat{r})$. We ignore sedimentation of the red blood cells, and assume the suspension has uniform mass density ρ. Under these conditions, the creeping flow equations reduce to,

$$\vec{\nabla} P = \vec{\nabla} \cdot \left(\eta_\phi(\hat{r}) \frac{\partial u}{\partial \hat{r}}\right),$$

$$\frac{dP}{dz} = \frac{1}{\hat{r}} \frac{d}{d\hat{r}} \left\{\hat{r}\left(\eta_\phi(\hat{r}) \frac{du}{d\hat{r}}\right)\right\}.$$

For constant pressure-driven flow, the velocity profile is calculated by integrating the preceding equation twice,

$$u(\hat{r}) = -\frac{1}{2}\left(\frac{dP}{dz}\right) \int_{\hat{r}}^1 \frac{\hat{r}'}{\eta_\phi(\hat{r}')} \, d\hat{r}'. \tag{7}$$

In the vessels of the body, the driving pressure is pulsatile,

$$-\frac{dP}{dz} = P_0(1 + \alpha \sin \omega t).$$

Assuming that in the small vessels the amplitude of the pressure pulse is small ($\alpha \ll 1$) so that $\phi^{ss}(\hat{r})$ remains approximately constant during each pulse, and assuming the Strouhal number R_ω is small,

$$R_\omega = \frac{\omega R^2 \rho}{\eta_0} \ll 1,$$

the pulsatile steady-state velocity profile is [27],

$$u(\hat{r}, t) = \frac{P_0(1 + \alpha \sin \omega t)}{2\eta_0} \left[\int_{\hat{r}}^{1} \frac{\eta_0 \hat{r}' d\hat{r}'}{\eta_\phi(\hat{r}')} \right]$$

$$-\frac{\alpha P_0 R_\omega}{2\eta_0} \left[\int_{\hat{r}}^{1} \int_{0}^{\hat{r}'} \int_{\hat{r}''}^{1} \frac{\eta_0^2 \hat{r}'' \hat{r}''' \, d\hat{r}''' d\hat{r}'' d\hat{r}'}{\hat{r}' \eta_\phi(\hat{r}') \eta_\phi(\hat{r}''')} \right] \cos \omega t.$$

3   Results

The effective viscosity of blood is often reported in experiments [22]. To make sense of this data, we must ask what is meant by the effective viscosity of a suspension; viscosity is a bulk property of homogeneous fluids, while suspensions are necessarily inhomogeneous. For example, in a capillary viscometer the flow rate Q is measured as a function of the pressure drop ΔP along the tube of length L . Assuming the fluid is homogeneous, and the flow is laminar, the effective viscosity is defined by the ratio

$$\eta_{\text{eff}} \equiv \frac{\pi}{8L} \frac{\Delta P}{Q},$$

and the flow rate is

$$Q = 2\pi \int_{0}^{1} \hat{r} u(\hat{r}) \, d\hat{r}. \tag{8}$$

Using the velocity distribution calculated above (Eq. 7), the effective viscosity η_{eff} becomes a function of the inhomogeneous Péclet number ε,

$$\eta_{\text{eff}} = \frac{1}{8} \left[\int_{0}^{1} \hat{r} \left\{ \int_{\hat{r}}^{1} \frac{\hat{r}' \, d\hat{r}'}{\eta_\phi(\hat{r}')} \right\} \, d\hat{r} \right]^{-1} \tag{9}$$

Clearly the effective viscosity is a particular kind of averaged local viscosity - particular to the type of viscometer being used. That is one of the reasons for the great variety of blood viscosity values reported in literature. The effective viscosity is not an intrinsic property of a suspension, but depends upon the underlying flow-induced microstructure and upon the averaging implicit in the instrument used to make the measurement.

In order to present explicit plots of $\eta_{\text{eff}}(\varepsilon), \phi^{ss}(\hat{r})$ and the resulting velocity distributions, we must choose an explicit form for the local suspension

viscosity $\eta_\phi(\hat{r})$. A common expression is [34, 4, 11, 25, 31],

$$\eta_\phi(\hat{r}) = \eta_0 \left(1 - \frac{\phi^{ss}(\hat{r})}{\phi_{\max}}\right)^{-T}, \tag{10}$$

where T is an empirical parameter characterizing the sensitivity of the viscosity to particle packing. Depending upon the choices of $\phi_{\max}$ and T, Eq. 10 reproduces the popular expressions of Roscoe [34], Brinkman [4], Dientenfass [11], and others [25, 31]. Note that Eq. 10 is generally derived in the context of homogeneous concentrated suspensions. In using the expression above, we assume that at each radial position $\hat{r}$, the suspension is a locally homogeneous Newtonian fluid. The non-Newtonian behaviour of the flow is then a result of the combined effect of each microscopic lamina on the overall suspension velocity (Figure 2).

Despite the general form of the local viscosity given by Eq. 10, certain features of the model can be made obvious by examining the small inhomogeneous Péclet number limit, $\varepsilon \to 0$. Substituting the general expression for the local viscosity $\eta_\phi(\hat{r})$, Eq. 10 and the general fluid flow $u(\hat{r})$ into the effective viscosity as measured by a capillary viscometer, η_{eff} (Eq. 9), retaining linear terms in the inhomogeneous Péclet number ε, we are able to calculate the effective viscosity of a nearly-homogeneous suspension flow of initial volume fraction ϕ_0,

$$\eta_{\text{eff}} \sim \eta_0 \left(1 - \frac{\phi_0}{\phi_{\max}}\right)^{-T} \left\{1 - \frac{\varepsilon T}{6} \frac{(\phi_0/\phi_{\max})}{(1 - \phi_0/\phi_{\max})} + \mathcal{O}(\varepsilon^2)\right\},$$

as $\varepsilon \to 0$. We see that the effect of the flow (*i.e.* $\varepsilon > 0$) is to reduce the effective viscosity (shear-thinning), and that this effect is most pronounced for suspensions near maximal packing density ($\phi_0 \approx \phi_{\max}$). In the dilute limit $\phi_0 \to 0$, we recover Einstein's relation with a correction due to the flow

$$\eta_{\text{eff}} \sim \eta_0 \left[1 + \frac{\phi_0}{\phi_{\max}} T \left\{1 - \frac{\varepsilon}{6}\right\}\right],$$

as $\varepsilon \to 0$ and $\phi_0 \to 0$. Furthermore, in the slow-flow limit the velocity profile given by Eq. 7 becomes,

$$u(\hat{r}) \sim -\frac{1}{4}\left(\frac{dP}{dz}\right)\frac{(1-\hat{r}^2)}{\eta_0(1-\phi_0/\phi_{\max})^{-T}} \left[1 + \frac{\varepsilon T}{2}\frac{\phi_0/\phi_{\max}}{(1-\phi_0/\phi_{\max})}\hat{r}^2 + \mathcal{O}(\varepsilon^2)\right],$$

as $\varepsilon \to 0$. The term proportional to ε represents a correction to the parabolic profile of homogeneous Poiseuille flow, and results in a blunt distribution along the axis.

To make contact with experimental results we must choose an explicit value for the maximum packing density $\phi_{\max}$ and the phenomenological exponent T. Red blood cells are quite flexible and several investigators have reported flow of concentrated suspensions ($\phi_0 > 0.95$). It seems reasonable,
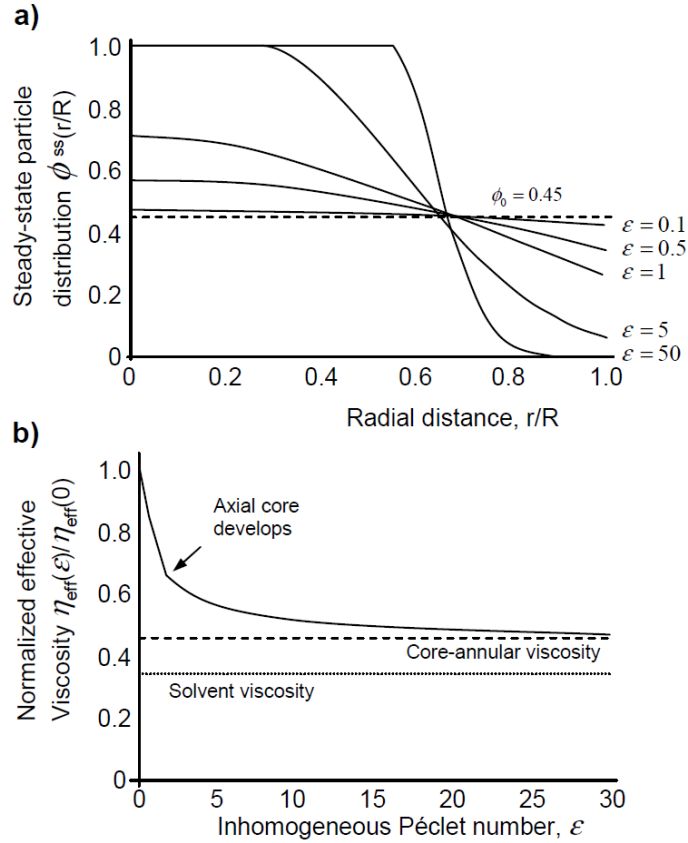
Figure 2: **Shear-thinning by particle migration**. a) The inhomogeneous Péclet number ε, Eq. 5, is a measure of the ratio of the flow-induced particle migration to the rate of diffusion. At steady-state, the convective and diffusive flux balance, resulting in a Gaussian particle distribution, with a densely packed particulate core surrounded by a cell-depleted region. Here, in the expression for the local viscosity $\eta_\phi(\hat{r})$ (Eq. 10), we have used $\phi_{\max} = 1$ and $T = 1.8$. b) Increasing the shear rate will increase the inhomogeneous Péclet number ε, so a suspension of deformable particles will display shear-thinning at low Reynolds number. In the limit of high Péclet number ε, the suspension behaves like a core-annular flow with the particles maximally packed along the axis surrounded by layer of pure solvent, and the effective viscosity is constant.

therefore, to set $\phi_{\max} = 1$ so that the viscosity stays finite for any physically accessible hematocrit. The exponent T is more open to interpretation. Experimental evidence suggests that T is around 2, but there is a great deal of variation from data set to data set [23]. We will choose the value $T = 1.8$ to remain consistent with the work of Krieger [25] and Phillips et al. [31]. Having fully specified the form of the local viscosity, we will apply the model in two ways. First, we shall treat the inhomogeneous Péclet number ε as a free parameter, using the model to reconstruct complete velocity profile information from a couple of data points, or from the experimental flow rate. Second, using the physical interpretation of the inhomogeneous Péclet number ε afforded by Eq. 5, we shall calculate the effective interfacial tension and the shear-dependent diffusion rate of red blood cells in tube flow.

3.1 Using the inhomogeneous Péclet number ε to fit incomplete data

Non-invasive measurement techniques such as magnetic resonance imaging (MRI) are being used to estimate the wall shear stress in physiological flow. Unfortunately, the spatial resolution of these techniques is limited, and sub-pixel data estimation is necessary, often with data near the wall fit to a paraboloid [30]. With the present model, using " as a free parameter, we can reconstruct missing data and estimate the wall shear stress. Figure 3a shows the velocity profile fitted to two data points half-way between the axis and the wall (filled circles). These data points and those shown as open circles are taken from the observed flow of a concentrated suspension of ghost red blood cells through a narrow glass tube (Figure 5 of [17]). The dashed line is the parabolic fit through the same two points. The inset shows that a parabolic fitting function underestimates the wall shear stress (which is proportional to $u'(r)$) by about 160%.

Alternatively, the inhomogeneous Péclet number ε can be determined by matching the model to the experimentally determined flow rate, via Eq. 8; the flow $u(\hat{r}; \varepsilon)$ will inherit a dependence on the Péclet number through the viscosity $\eta_\phi(\hat{r})$. Integrating over the cross-section of the tube, we obtain the flow-rate as a function of the inhomogeneous Péclet number ε, $Q(\varepsilon)$. Comparing $Q(\varepsilon)$ to the experimental flow rate $Q_{\exp}$, we are able to determine the choice of Péclet number ε that will reproduce the observed flow rate. With ε so determined, we plot the complete flow $u(r; \varepsilon)$, and the velocity profile is reconstructed exactly (Figure 3b). Here again the data points (filled circles) are taken from ghost cell flow through glass tubes (Figure 5 of [17]). Note that the profile $u(r; \varepsilon)$ is not fit to the data points the Péclet number ε is simply chosen to match the spatially-averaged flow rate Q. The close agreement between the model and data lends credence to the mathematical form of the velocity function.
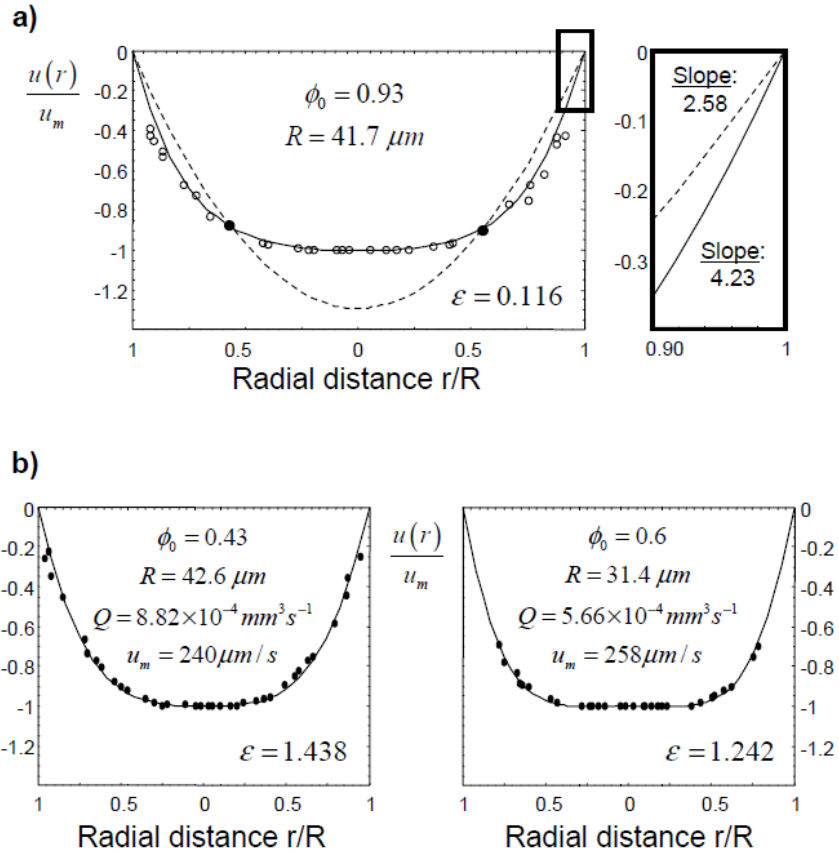
a)

b)

Figure 3: **Reconstruction of the flow velocity profile from incomplete data**. a) Estimating the wall shear stress: The Péclet number ε is determined by fitting the velocity profile to two points (filled circles). The missing data is shown as open circles. *Inset:* The parabolic fit (dashed) underestimates the wall shear stress by a factor of 1.6. b) Estimating the velocity profile from the experimental flow rate: Given the centerline velocity u_m, the hematocrit ϕ_0 and the tube radius R the Péclet number ε is chosen so that model flow rate Q (Eq. 8) matches the experimental flow rate Q_{exp}. Here the velocity data is shown as filled circles. The model is able to accurately predict the complete velocity profile (Eq. 7; solid line). All data is from [17] for ghost red cells flowing through glass tubes.
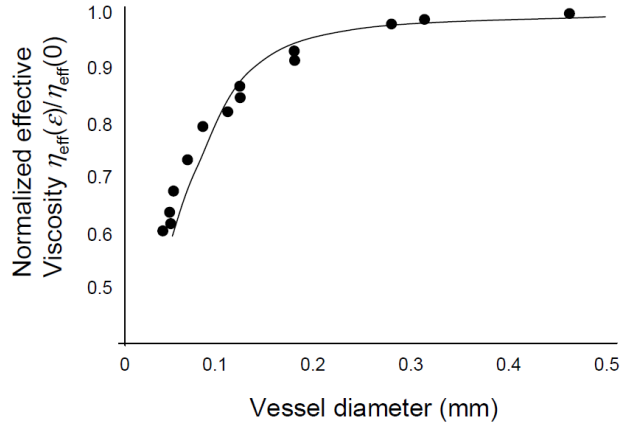
Figure 4: **The Fahraeus-Lindqvist effect**. The original data of Fahraeus and Lindqvist [13] is shown as filled circles, with the limiting viscosity normalized to one. The Péclet number ε is proportional to R^{-2}, and the effective viscosity η_{eff}, Eq. 9, calculated with $\varepsilon = 0.2R^{-2}$ (R measured in mm) is shown as a solid line.

3.2 The Fahraeus-Lindqvist effect

The definition of the inhomogeneous Péclet number ε, Eq. 5, allows the reproduction of the anomalous flow behavior of blood by fixing various combinations of physical parameters. For example, we see that for a given experimental set-up the Péclet number is inversely-proportional to the squared vessel radius, $\varepsilon \propto R^{-2}$. Fitting the original data of Fahraeus and Lindqvist [13] normalized to unity, we can fix the proportionality constant,

$$\varepsilon = \frac{0.2}{R^2},$$

with the tube radius R measured in mm. The resulting fit to the experimental data using the effective viscosity given by Eq. 9 is shown in Figure 4.

3.3 Determining the inhomogeneous Péclet number ε from physical data

The definition of the inhomogeneous Péclet number ε is given in terms of physical parameters (Eq. 5) and should in principle allow rheological data to be predicted. There is, however, some difficulty assigning meaning to the constants V_{max} and D, along with the interfacial tension σ appearing in the definition.

The migration velocity f_u, Eq. 3, was derived by Chan and Leal in terms of the motion of a single drop in a unidirectional flow, so the background
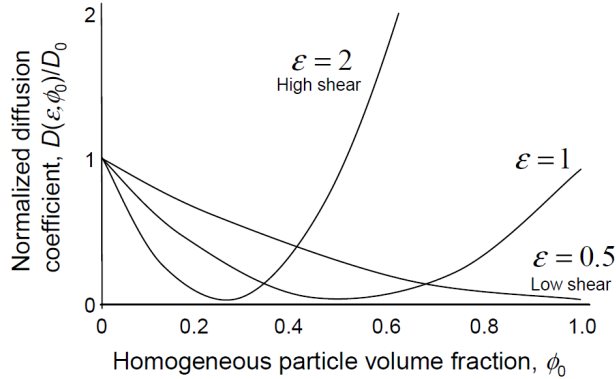
Figure 5: **Effect of shear and particle packing on the flow-dependent diffusion rate** $D(\varepsilon, \phi_0)$.   The flow-dependent diffusion rate coefficient $D(\varepsilon, \phi_0) = D_0(1 - 3.77\varepsilon\phi_0 + 3.7\varepsilon^2\phi_0^2)$, is dominated by cage effects at low shear ($\varepsilon < 0.5$) where close packing restricts diffusion. As the shear rate increases ($\varepsilon \geq 2$), asymmetric collisions among particles enhance the diffusion rate in concentrated suspensions.

flow will not be affected by the motion of the drop. For a concentrated suspension, redistribution of the particles by the background flow will change the suspension flow geometry in an essential way. In particular, the maximum flow velocity along the axis u_m is no longer related to the shear gradient near the wall via Poiseuille's law and therefore cannot be identified as $V_{\max}$ in the migration velocity f_u. Nevertheless, in the vicinity of the wall where drop migration is dominant we can determine the parabolic contribution to the shear gradient by taking a Taylor expansion of the suspension velocity profile $u(\hat{r}; \varepsilon)$ (Eq. 7) about the vessel edge $\hat{r} = 1$, retaining quadratic terms, to find

$$V_{\max} = \frac{u_m}{2\eta_\phi(1) \int_0^1 \frac{\hat{r}' d\hat{r}'}{\eta_\phi(\hat{r}')}}$$

In this way, we are able to connect the centerline velocity u_m to the mean-field shear gradient that an individual particle will experience near the wall, and hence calculate the cross-stream migration velocity. With $V_{\max}$ expressed in terms of experimentally accessible quantities, the remaining parameters D and σ are left to fully characterize the Péclet number ε.

   Diffusion of an individual particle in a concentrated suspension is enhanced by the flow (shear-induced diffusion [24, 28]) and constrained by the close-packing of neighboring particles (cage effects [10]). In general, these contributions will not be uniform across the vessel, but as a first approximation we consider the diffusion coefficient D as a spatially homogeneous function of the Péclet number ε (characterizing the flow) and ϕ_0 (characteriz-

ing the average packing fraction). For simplicity, we assume a polynomial in the Péclet number ε and ϕ_0. The inhomogeneous Péclet number ε can be fit to flow rate data (see Fig. 3), we will use the data of Glodsmith and Marlow to determine $D(\varepsilon, \phi_0)$ such that the variance in the estimate of the interfacial surface tension σ is minimized across the data sets. Data is taken from Figure 5 of [17], excluding Figure 5b (right) because the tube Reynolds number is too large. To ensure that the suspension flow is adequately modeled by the creeping flow equations, we require that the tube Reynolds number $\mathrm{Re} = 2u_m R\rho/\eta_0$ be less than 0.05, $\mathrm{Re} \ll 0.05$, where ρ is the plasma density ($\rho \approx 1030$ kg m^{-3}). Considering a second-order polynomial fitting function, we arrive at the flow-dependent diffusion constant

$$D(\varepsilon, \phi_0) = D_0(1 - 3.77\varepsilon\phi_0 + 3.7\varepsilon^2\phi_0^2),$$

where D_0 is the Einstein-Stokes diffusion coefficient,

$$D_0 = \frac{kt}{6\pi\eta_0 a}.$$

Here k is Boltzmann's constant and t is the absolute temperature. The form of the fitting function is justified by examining the effect of velocity fluctuations in the particle conservation equation arising from red cell-red cell collisions [35]. Qualitatively, the diffusion constant $D(\varepsilon, \phi_0)$ behaves as one would hope (Figure 5): As the shear-rate increases, shear-induced diffusion overcomes cage effects, increasing the apparent rate of diffusion. With this choice of $D(\varepsilon, \phi_0)$, the resulting estimate for the interfacial surface tension σ is,

$$\sigma = (1.2 \pm 0.1) \times 10^{-4}\mathrm{N\ m}^{-1},$$

as determined from the data of five experiments. Although within this model the red blood cells behave like deformable droplets with interfacial tension $\sigma = 1.2 \times 10^{-4}\mathrm{N\ m}^{-1}$, in reality the cells are biconcave disks with a cell-membrane tension of about 10^{-5} N m^{-1} [12], an order of magnitude less than the model estimate. It is important to note that the internal architecture of the cell and the membrane itself lend an apparent rigidity opposing cell deformation not found in a simple fluid drop.

Collecting the estimates for $V_{\max}(\varepsilon, \phi_0)$ and the diffusion coefficient $D(\varepsilon, \phi_0)$, we arrive at an implicit nonlinear equation for the inhomogeneous Péclet number ε,

$$\varepsilon = \frac{11}{140} \frac{V_{\max}^2(\varepsilon, \phi_0)}{\sigma} \frac{\eta_0 a}{D(\varepsilon, \phi_0)} \left(\frac{a}{R}\right)^2.$$

Here, the effective interfacial tension $\sigma = 1.2 \times 10^{-4}$ N m^{-1}, the nominal plasma viscosity is $\eta_0 = 1.1 \times 10^{-3}$kg m^{-1}s^{-1}, and the deformed red cell radius $a = 3.5 \times 10^{-6}$m. The hematocrit ϕ_0, vessel radius R and centerline velocity u_m depend upon the details of the particular system under investigation. To test the many simplifications made to develop an expression for

the flow-dependent diffusion coefficient $D(\varepsilon, \phi_0)$ and fix the effective interfacial tension σ, we compare the theoretically predicted velocity profile to independent experimental data not used in the fitting procedure.

The *in vitro* data of Goldsmith and Turrito (Figure 2 of Ref. [18]) for concentrated ghost cells in glass tubes is shown in Figure 6a. The experimental parameters are $\phi_0 = 0.52$, $R = 51.8\mu$m and $u_m = 360\mu$m/s. This is all the information required to estimate the velocity profile across the tube, and the theoretical prediction fits the data well.

In vivo data is far more difficult to collect, and human data is scarce. Nonetheless, making use of the excellent data of Sugii *et al.* (Figure 7d of Ref. [37]) for blood flowing in the small arterioles of a rat, with $R = 12\mu$ m, $u_m = 3.1$mm/s and estimated rat hematocrit $\phi_0 = 0.45$ [41], we again find good agreement between the experimental results and the theoretical prediction (Figure 6b).

It is important to note that no free parameters are used to improve the fit of the model in Fig. 6. The agreement in both the ghost-cell/glass tube case (Fig. 6a) and the red blood cell/*in vivo* vessel case (Fig. 6b), using the same model with no additional fit parameters suggests that the phenomenological approach is useful beyond the ghost cell/galss tube data used to parameterize the model.

4   Conclusion and outlook

Applying the results of Chan and Leal [6] describing the motion of a deformable droplet in unidirectional creeping flow, we are able to derive a predictive model that describes the steady-state velocity profile and measured effective viscosity of a suspension of deformable particles, with particular application to the modeling of blood. The model behaviour is characterized by a single parameter, ε, that acts as a Péclet number for the suspension of deformable particles in tube flow.

Using the inhomogeneous Péclet number ε to fit the experimental flow rate of ghost red blood cells through a glass tube, we are able to reproduce the velocity field exactly (Fig. 3). With an empirical choice of the diffusion rate coefficient, chosen to minimize the value of the apparent interfacial tension σ of the model droplets as compared to the data of Goldsmith and Marlow [17], we arrive at a quantitative, predictive model for blood rheology that requires only the hematocrit ϕ_0, the vessel radius R and the centerline velocity u_m to calculate the velocity field and effective viscosity of the suspension flow.

The present model is derived under the assumption of vanishingly small Reynolds number Re $= 2u_m R\rho/\eta_0 \ll 0.05$, though for more rapid flow, inertial effects become important. Macroscopically, these effects appear as an increase in the effective viscosity and a decrease in the blunting of the velocity profile near the vessel axis [16]. Microscopically, in keeping with the observations of Segre and Silberberg [36], the particles will move away from
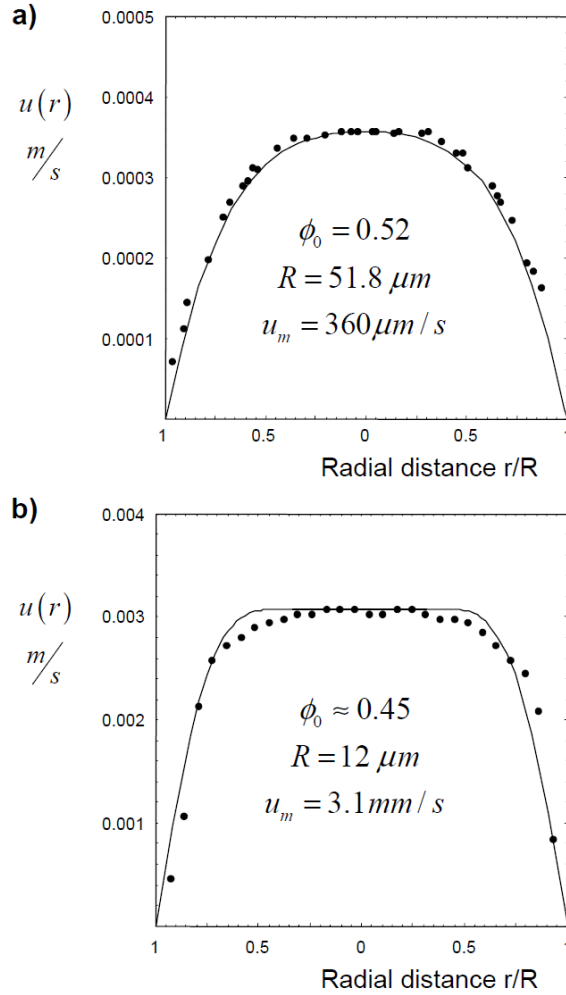
a)

$u(r)$

m/s

$$\phi_0 = 0.52$$

$$R = 51.8\,\mu m$$

$$u_m = 360\,\mu m/s$$

Radial distance r/R

b)

$u(r)$

m/s

$$\phi_0 \approx 0.45$$

$$R = 12\,\mu m$$

$$u_m = 3.1\,mm/s$$

Radial distance r/R

Figure 6: **Parameterless-fit of the model to experimental data**. a) The model prediction is shown along with the *in vitro* data for the flow of ghost red blood cells through glass tubes [18]. b) The data is for the flow of rat's blood through an arteriole [37]. The hematocrit is not reported, but we estimate $\phi_0 = 0.45$ [41].

the axis. To leading order, the effects of inertia and particle deformation are additive in the migration velocity [26] and including both mechanisms in the convective flux would extend the range of the model to larger Reynolds number flow.

5 Acknowledgements

References

[1] M. Arakawa, T. Kondo and B. Tamamushi, Flow properties of microcapsule suspensions as a model of blood, *Biorheology*, **12**, (1975) 57-66.

[2] G. K. Batchelor. Developments in microhydrodynamics. In W. T. Koiter, editor, *Theoretical and applied mechanics*. North-Holland (1976) pp. 33-35.

[3] F. P. Bretherton, The motion of rigid particles in a shear flow at low Reynolds number, *Journal of Fluid Mechanics*, **14**, (1962) 284-304.

[4] H. C. Brinkman, The viscosity of concentrated suspensions and solutions, *Journal of Chemical Physics*, **20**, (1952) 571.

[5] N. Casson. A flow equation for pigment-oil suspensions of the printing ink type. In C. C. Mill, editor, *Rheology of disperse systems*. Pergamon Press (1959) pp. 84-104.

[6] P.C.-H. Chan and L. G. Leal, Motion of a deformable drop in a second-order fluid, *Journal of Fluid Mechanics*, **92**, (1979) 131-170.

[7] S. E. Charm and G. S. Kurland, Blood flow and microcirculation, John Wiley and Sons, Inc., New York, 1974.

[8] S. Chien,Shear dependence of effective cell volume as a determinant of blood viscosity, *Science*, **168**, (1970) 977-979.

[9] T. S. Chow, Mesoscopic physics of complex materials, Springer-Verlag, Berlin, 2000.

[10] E. G. D. Cohen and I. M. deSchepper, Transport properties of concentrated colloidal suspensions. In T. Kawakatsu K. Kawasaki and M. Tokuyama, editors, *Slow dynamics in condensed matter*, American Institute of Physics (1992), pp. 359-369.

[11] L. Dientenfass, Internal viscosity of the red cell and a blood viscosity equation, *Nature*, **219**, (1968) 956-958.

[12] E. Evans, N. Mohandas and A. Leung, Static and dynamic rigidities of normal and sickle erythrocytes, *Journal of Clinical Investigation*, **73** 477-488.

[13] R. Fahraeus and T. Lindqvist, Viscosity of blood in narrow capillary tubes, *American Journal of Physiology*, **96**, (1931) 562-568.

[14] F. J. Gauthier, H. L. Goldsmith, and S. G. Mason, Flow of suspensions through tubes. X. Liquid drops as models of erythrocytes, *Biorheology*, **9**, (1972) 205-224.

[15] J. D. Goddard and C. Miller, Nonlinear effects in the rheology of dilute suspensions, *Journal of Fluid Mechanics*, **28**, (1967) 657-673.

[16] H. L. Goldsmith, The microrheology of human blood, *Microvascular Research*, **31**, (1986) 121- 142.

[17] H. L. Goldsmith and J. C. Marlow, Flow behavior of erythrocytes. II. Particle motions in concentrated suspensions of ghost cells, *Journal of Colloid and Interface Science*, **71**, (1979) 383-407.

[18] H. L. Goldsmith and V. T. Turrito, Rheological aspects of thrombosis and haemostasis: Basic principles and applications, *Thrombosis and Haemostasis*, **55**, (1986) 415-435.

[19] B. B. Gupta, K. M. Nigam and M. Y. Jaffrin, A three-layer semi-empirical model for flow of blood and other particulate suspensions through narrow tubes, *Journal of Biomechanical Engineering*, **104**, (1981) 129-135.

[20] R. Herczynski and I. Pienkowska, Toward a statistical theory of suspension, *Annual Review of Fluid Mechanics*, **12**, (1980) 237-269.

[21] S. D. Hudson, Wall migration and shear-induced diffusion of fluid droplets in emulsions, *Physics of Fluids*, **15**, (2003) 1106-1113.

[22] International committee for standardization in haematology (ICSH), Guidelines for measurement of blood viscosity and erythrocyte deformability, *Clinical Hemorheology*, **6**, (1986) 439-453.

[23] D. J. Jeffrey and A. Acrivos, The rheological properties of suspensions of rigid particles, *American Institute of Chemical Engineers Journal*, **22**, (1976) 417-432.

[24] M. R. King and D. T. Leighton, Measurement of shear-induced dispersion in a dilute emulsion, *Physics of Fluids*, **13**, (2001) 397-406.

[25] I. M. Krieger, Rheology of monodisperse lattices, *Advances in Colloid and Interface Science*, **3**, (1972) 111-136.

[26] L. G. Leal, Particle motions in a viscous fluid, *Annual Review of Fluid Mechanics*, **12**, (1980) 435-476.

[27] L. G. Leal, Laminar flow and convective transport processes, Butterworth-Heinemann, Boston, 1992.

[28] D. Leighton and A. Acrivos, The shear-induced migration of particles in concentrated suspensions, *Journal of Fluid Mechanics*, **181**, (1987) 415-439.

[29] R. G. Owens, A new microstructure-based constitutive model for human blood, *Journal of Non-Newtonian Fluid Mechanics*, **140**, (2006) 57-70.

[30] S. Oyre, S. Ringgaard, S. Kozerke, W. P. Paaske, M. B. Scheidegger, P. Boesiger, and E. M. Pedersen, Quantitation of circumferential subpixel vessel wall position and wall shear stress by multiple sectored three-dimensional paraboloid modeling of velocity encoded cine-MR, *Magnetic Resonance in Medicine*, **40**, (1998) 645-655.

[31] R. J. Phillips, R. C. Armstrong, R. A. Brown, A. L. Graham and J. R. Abbot, A constitutive equation for concentrated suspensions that accounts for shear-induced particle migration, *Physics of Fluids A*, **4**, (1992) 30-40.

[32] C. Pozrikidis, Boundary integral and singularity methods for linearized viscous flows, Cambridge University Press, Cambridge, 1992.

[33] M. Reiner and G. Scott-Blair, The importance of the sigma phenomenon in the study of the flow of blood, *Rheologica Acta*, **1** (1958).

[34] R. Roscoe, The viscosity of suspensions of rigid spheres, *British Journal of Applied Physics*, **3**, (1952) 267-269.

[35] M. Scott, The modeling of blood rheology in small vessels, PhD Thesis, University of Waterloo, Waterloo Canada May 2005: available at https://uwspace.uwaterloo.ca/bitstream/handle/10012/1149/mscott2005.pdf;sequence=1

[36] G. Segre and A. Silberberg, Behaviour of macroscopic rigid spheres in poiseuille flow. Part 2 - Experimental results and interpretation, *Journal of Fluid Mechanics*, **14**, (1962) 136- 157.

[37] Y. Sugii, S. Nishio and K. Okamoto, In vivo PIV measurement of red blood cell velocity field in microvessels considering mesentery motion, *Physiological Measurement*, **23**, (2002) 403- 416.

[38] C. Sun and L. L. Munn, Particulate nature of blood determines macroscopic rheology: A 2-D lattice Boltzmann analysis, *Biophysical Journal*, **88**, (2005) 1635-1645.

[39] G. I. Taylor, The viscosity of a fluid containing small drops of another fluid, *Proceedings of the Royal Society (London)*, **138A**, (1932) 41-48.

[40] E. G. Tickner and A. H. Sacks, Engineering simulation of the viscous behavior of whole blood using suspensions of flexible particles, *Circulatory Research*, **25**, (1969) 389-400.

[41] U. Windberger, A. Bartholovitsch, R. Plasenzotti, K. J. Korak and G. Heinze, Whole blood viscosity, plasma viscosity and erythrocyte aggregation in nine mammalian species: Reference values and comparison of data, *Experimental Physiology*, **88**, (2003) 431- 440.